Nuclear Instruments and Methods in Physics Research A 712 (2013) 15–26

Contents lists available at SciVerse ScienceDirect

Nuclear Instruments and Methods in Physics Research A

journal homepage: www.elsevier.com/locate/nima

# LUPIN, a new instrument for pulsed neutron fields

M. Caresana [a], M. Ferrarini [a,b], G.P. Manessi [c,d,*], M. Silari [c], V. Varoli [a]

[a] Politecnico di Milano, Department of Energy, Via Ponzio 34/3, 20133 Milan, Italy
[b] CNAO, Via Privata Campeggi, 27100 Pavia, Italy
[c] CERN, 1211 Geneva 23, Switzerland
[d] University of Liverpool, Department of Physics, L69 7ZE Liverpool, UK

ARTICLE INFO

*Article history:*
Received 15 October 2012
Received in revised form
21 January 2013
Accepted 21 January 2013
Available online 15 February 2013

*Keywords:*
$^3$He
Neutron detection
Pulsed field
Linac
Proportional counter
Logarithmic amplifier

ABSTRACT

A number of studies focused in the last decades on the development of survey meters to be used in pulsed radiation fields. This is a topic attracting widespread interest for applications such as radiation protection and beam diagnostics in accelerators. This paper describes a new instrument specifically conceived for applications in pulsed neutron fields (PNF). The detector, called LUPIN, is a rem counter type instrument consisting of a $^3$He proportional counter placed inside a spherical moderator. It works in current mode with a front-end electronics consisting of a current–voltage logarithmic amplifier, whose output signal is acquired with an ADC and processed on a PC. This alternative signal processing allows the instrument to be used in PNF without being affected by saturation effects. Moreover, it has a measurement capability ranging over many orders of burst intensity. Despite the fact that it works in current mode, it can measure a single neutron interaction. The LUPIN was first calibrated in CERN's calibration laboratory with a PuBe source. Measurements were carried out under various experimental conditions at the Helmholtz-Zentrum in Berlin, in the stray field at various locations of the CERN Proton Synchrotron complex and around a radiotherapy linear accelerator at the S. Raffaele hospital in Milan. The detector can withstand single bursts with values of H*(10) up to 16 nSv/burst without showing any saturation effect. It efficiently works in pulsed stray fields, where a conventional rem-counter underestimates by a factor of 2. It is also able to reject the very intense and pulsed photon contribution that often accompanies the neutron field with good reliability.



## 1. Introduction

The need of radiation detectors capable to measure efficiently in PNF.[1] is attracting widespread interest for applications such as radiation protection and beam diagnostics in accelerators. Since the 60s, numerous investigations focused on the development of detectors specifically conceived to work in pulsed fields [1–3]. This is a major issue at particle accelerators, where pulsed neutron and gamma fields are present because of beam losses at e.g. targets, collimators and beam dumps. It is well-known that conventional detectors generally suffer from dead time effects and have strong limitations in the measurements of pulsed fields. Severe under response has been observed in commercial rem counters [4], with tremendous underestimation of the ambient dose equivalent, H*(10), up to three orders of magnitude [5].

An ideal neutron survey meter for PNF should meet the following requirements:

1. capability to withstand very high instantaneous neutron fluxes with little or no saturation;
2. sensitivity comparable to that of commercially available rem counters;
3. capability to measure correctly the intensity of a single neutron burst and
4. capability to reject the photon contribution that accompanies the neutron field.

For use in high-energy fields like those encountered around particle accelerators or cosmic-ray fields, a good sensitivity to high-energy neutrons is also desirable.

One way to deal with the problem of PNF is to use an activation detector and there has been extensive research in this fields since the 70s [6,7]. A considerable effort has recently been made on the improvement of silver-activation detectors [8,9], for which experiments have shown good linearity in pulsed fields [9].

* Corresponding author at: CERN, 1211 Geneva 23, Switzerland. Tel.: +41 764 879634.
*E-mail address:* giacomo.paolo.manessi@cern.ch (G.P. Manessi).

[1] PNF=Pulsed neutron fields.

0168-9002/$ - see front matter © 2013 Elsevier B.V. All rights reserved.
http://dx.doi.org/10.1016/j.nima.2013.01.060

This detector has low neutron sensitivity, around 9 counts per μSv for a bare $^{252}$Cf source [10]. Moreover, a neutron dose equivalent of 10 μSv is only measurable in a reliable way if the photon contribution is a factor of 10 lower [9]. However, the crucial issue of this detector is the response time, which is determined by the half-life of the Ag isotopes. This leads to a delayed response and rules out the detector from all potential applications with the need of an on-line response. The approach based on activation detectors eventually fulfills the requirements 1 and 4 above, but does not permit to measure the intensity of the single neutron burst. Moreover the sensitivity is about two orders of magnitude worse than commercially available rem counters.

Weizhen et al. [11] reported a way of reducing the counting losses of a neutron detector in PNF. Their method takes into account the nearly simultaneous detection of 2 or 3 neutrons in a proportional counter. However, they set a limit of 100 on the number of counts that each neutron burst produces in the counter and a limit of 0.1 Gy/h on the gamma dose rate that accompanies the neutron field. The limit on the number of counts is very stringent and does not allow the detector to meet the requirements 1 and 3 above. Klett et al. [12] developed a new survey meter designed to work in pulsed fields, based on the activation of $^{12}$C. The instrument has limited applications as can only be used for detecting neutrons above 20 MeV, and has strong limitations in sensitivity and on the burst repetition rate over which it can be used [4]. Consequently, the requirements 1 and 2 cannot be fulfilled. Leake et al. [4] proposed a method of measuring PNF based on the exploitation of the die-away of thermalized neutrons. However, at present there are no experimental results to support the theoretical basis. Very recently Iijima et al. [13] reported on the development of a current-readout type neutron monitor designed to measure the dose rate of neutrons bursts generated by beam losses in an accelerator. This monitor shows no count losses in a dynamic range from 4 μSv/h to 5 mSv/h. On the other hand, the monitor cannot distinguish a gamma signal from a neutron signal. Therefore the detector cannot operate under stringent constraints and the requirements 1 and 4 above cannot be respected.

This brief review shows that there is no device presently capable of fulfilling all the requirements listed above for PNF instruments. A promising approach is described by Ferrarini et al. [14], who have discussed the development of a wide dynamic range neutron monitor using a $BF_3$ proportional counter. This monitor works in current mode and has a front-end electronics based on a logarithmic amplifier. This allows having a measurement capability ranging over many orders of burst intensity. Despite the fact that it works in current mode, the detector can measure a single neutron interaction. This characteristic assures a sensitivity comparable to that of commercially available rem counters for steady neutron fields. On the other hand the detector is able to withstand reactions rates in the order of $10^6$ s$^{-1}$ without showing any saturation effect. The capability to reject the photon contribution accompanying the neutron field is still under investigation.

The prototype instrument which is the subject of this paper is called LUPIN (Long interval, Ultra-wide dynamic, PIle-up free, Neutron rem counter) and is an improved version of the detector proposed by Ferrarini et al. [14]. The device consists of a Centronics $^3$He-proportional counter, a spherical moderator and a front-end electronics based on a logarithmic amplifier. This paper describes the instruments and discusses the results of a number of measurements performed under various experimental conditions:

- calibration measurements with a PuBe source to evaluate the behavior in a steady neutron field;
- measurements in PNF produced with a cyclotron at the Helmholtz-Zentrum in Berlin to evaluate the response with a negligible photon field contribution;
- measurements in the stray field around the proton synchrotron (PS) accelerator complex at CERN, to compare the performance with those of other instruments in operational radiation protection conditions and
- measurements around a radiotherapy linear accelerator (linac) at the S. Raffaele hospital in Milan to evaluate the behavior in PNF dominated by a very intense photon component.

**Fig. 1.** A picture of the LUPIN. The $^3$He counter is electrostatically shielded with an aluminum tube connected to the electronics case. It is inserted in the spherical moderator from the top. The sphere is placed on a small iron pedestal.

## 2. Material and methods

### 2.1. The LUPIN

The LUPIN is a rem counter type instrument consisting of a $^3$He proportional counter placed inside a spherical moderator (see Fig. 1). The front-end electronics consists of a current–voltage logarithmic amplifier, whose output signal is acquired with an ADC and processed with a LabVIEW© program running on a personal computer. The idea of the analysis software is simple: the voltage signal is converted back into a current signal and integrated over a time that can be set by the user. The result of this calculation represents the total charge generated in the $^3$He detector by the neutron interaction. This quantity, divided by the average charge expected by a single neutron interaction, represents the number of neutron interactions occurring during the integration time.

### 2.2. Moderator

The moderator is designed so that the response function of the instrument reproduces sufficiently well the curve of the conversion coefficients from neutron fluence to H*(10) over a wide energy range, as in the original extended-range rem counter LINUS (Long Interval NeUtron Survey meter) [15]. The moderator consists of a polyethylene sphere of 12.5 cm outer radius with lead and cadmium inserts, hosting at its center the $^3$He proportional counter. The inner part of the moderator, 5.6 cm in radius, is surrounded by a 6 mm thick lead shell. The outer layer of this inner polyethylene sphere hosts eleven cadmium buttons, 2.5 cm in radius and 1 mm thick. Polyethylene inserts ("plugs") are used to fill the void around the detector stem. A scheme and a photograph of the inner parts of the rem counter are shown in Fig. 2. The spherical geometry of the moderator was adopted to make the monitor response isotropic. The problem related to the anisotropy of the geometry is in fact serious when monitoring neutrons fields whose angular distribution is unknown, and it can lead to an underestimation of the ambient dose equivalent [16,17].

The same spherical moderator has been used with CR39 dosimeters and a $^3$He proportional counter as a dual-detector extended-range rem counter (conventional, i.e. for non-pulsed fields) by Agosteo et al. [18]. The only difference is the electrostatic shield that contains the detector and the polyethylene plug. This shield is an aluminum cylinder of 1 mm thickness, which is inserted in the sphere together with the detector and the plug. The thickness of the polyethylene plug was reduced by the same thickness of the aluminum shield. The presence of this thin shield is not expected to alter the response function of the rem counter: the sensitivity has been checked and shown to be the same with or without this element, which is a good indicator that the response should also not be influenced. This will be confirmed by a further study. The aluminum electrostatic shield is needed because of the characteristic of the front end electronic as described below.

### 2.3. Proportional counter

The natural choice of the detector with respect to the spherical geometry of the moderator was a spherical Centronic SP9 $^3$He proportional counter. Although the $^3$He filling pressure is nominally stated as 2 atm (202,650 Pa), the actual pressure is 2.3 atm (233,047 Pa), to which 1.2 atm (121,590 Pa) of Krypton is added as a quench gas [19]. Another possible choice is a cylindrical $BF_3$ proportional counter. Although less isotropic, such an alternative can be attractive because of the higher $Q$-value of the $^{10}B(n, \alpha)^7Li$ reaction. The characterization of the version of the LUPIN with a $BF_3$ counter is presently under way and will be the subject of a forthcoming paper.

### 2.4. Electronics

The scheme of the front-end electronic is shown in Fig. 3. The polarization between the electrodes of the $^3$He counter is provided by a user-adjustable internal high voltage supply. The electronics is based on a current-voltage logarithmic amplification of the signal produced inside the proportional counter. A fixed current $I_{min}$ is added to the current signal $I_R$ generated by the reactions inside the counter to avoid negative saturation in case of absence of a neutron signal. This current is set to 200 pA, but this value can be modified if necessary. A larger value of $I_{min}$ causes a faster response of the LogAmp. The sum of the two currents, $I_R+I_{min}$, is collected and processed by the LogAmp. Because the signal is collected at the cathode, the proportional counter must be electrostatically shielded in order to avoid noise pick up. The electrostatic shield is made of an aluminum cylinder that completely encases the counter, as discussed above.

The LogAmp output signal passes through a cable driver and the signal $V_{LogOut}$ is acquired via a digital oscilloscope. For the measurements described in this paper the signal was acquired via a PC oscilloscope (PicoScope 4424 by PicoTechnology) and monitored by a LabVIEW© program running on a PC. More details about the theoretical operating principles of the circuit with explicit reference to the Kirchoff's laws and the Ebers–Moll equations can be found in Ref. [14]. The choice of a LogAmp was driven by the need to achieve a dynamic range of a few orders of magnitude with respect to the burst intensity to be measured. Conventional LogAmps are too slow for the purpose of the detection of a radiation signal, especially in the tail of the signal. It was then decided to employ a high-speed LogAmp. The attention was focused on two models, the AD8304 (Analog Devices) and the LOG114 (Texas Instrument). Both are

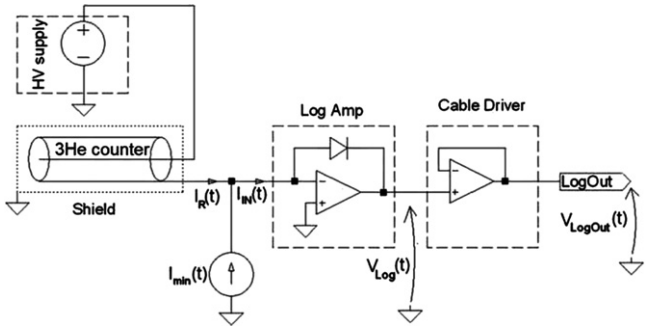


**Fig. 3.** General scheme of the detector electronics.

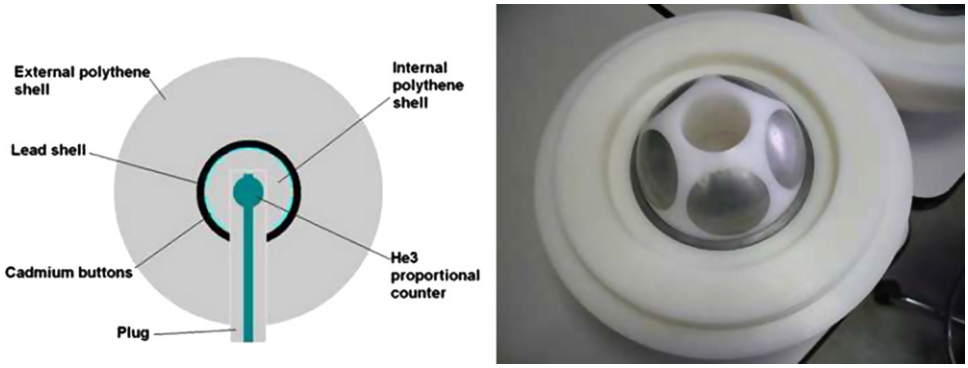


**Fig. 2.** Scheme of the detector and moderator assembly of the LUPIN and photograph of its inner part showing the inner polyethylene with the cadmium buttons, the lead shell and the outer polyethylene.

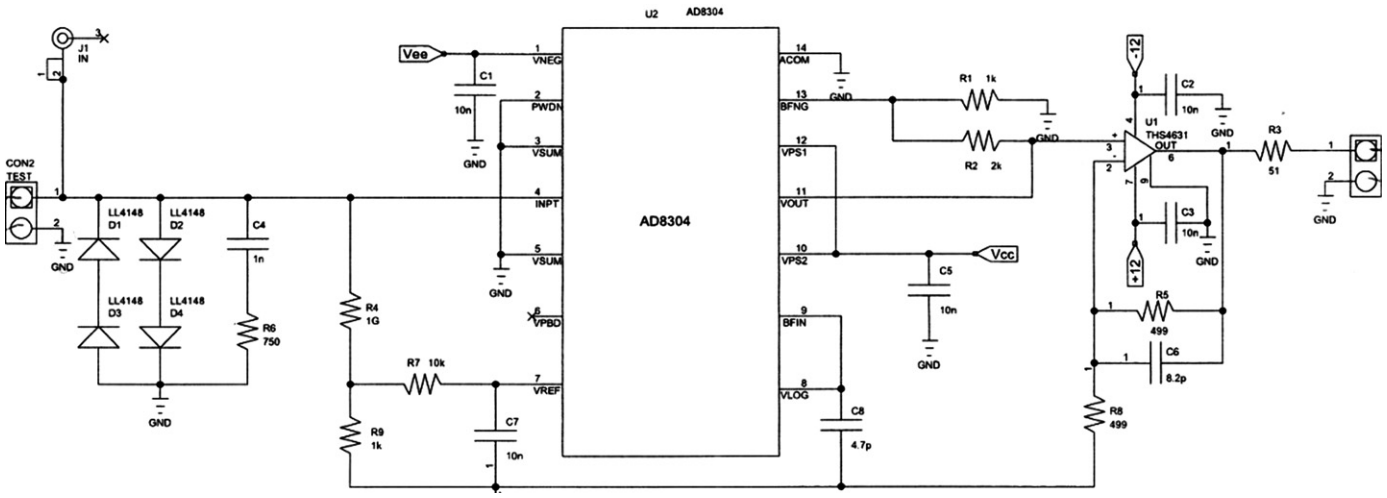


**Fig. 4.** Circuital scheme of the front-end electronics with the AD8304 LogAmp.

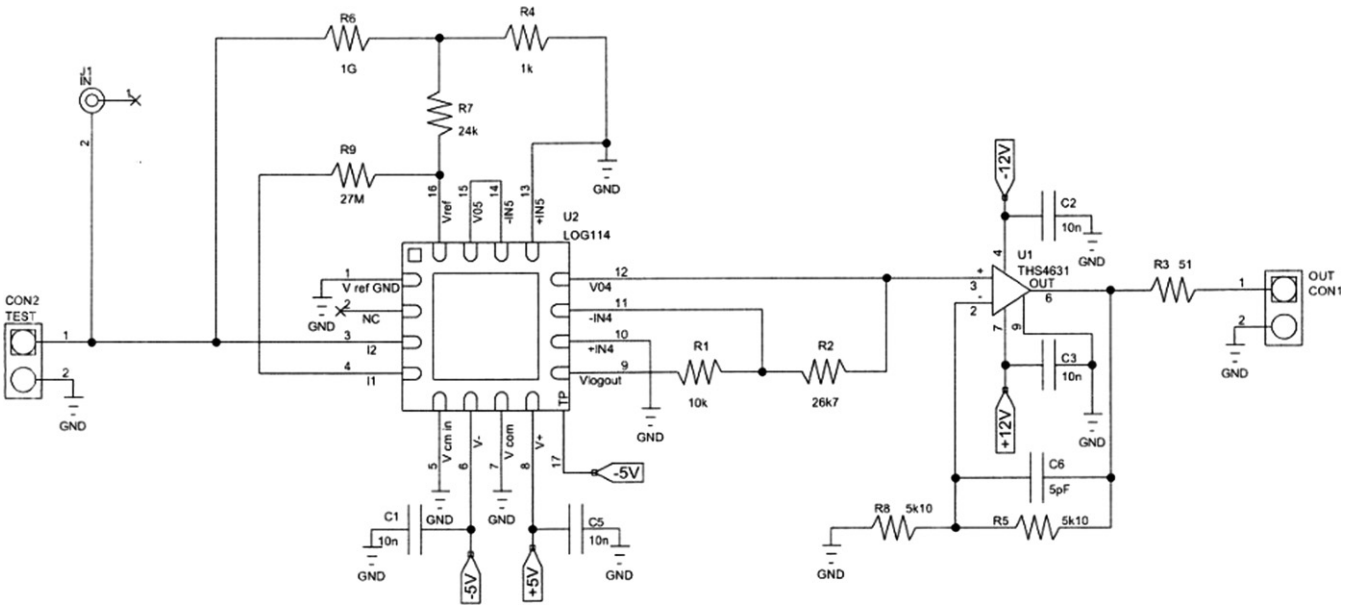


**Fig. 5.** Circuital scheme of the front-end electronics with the LOG114 LogAmp.

declared by the manufacturers to work over a range of eight decades (160 dB) with high temperature stability. The circuital schemes of the front-end electronics with the two LogAmps are shown in Figs. 4 and 5.

A number of tests were carried out to compare the performances of the two LogAmps. The attention focused on the different response of the LogAmps to the same input signals to better understand their functioning dynamics. Fig. 6 shows the response of the two LogAmps to the same input. The input current signal was generated applying a triangular voltage signal by a Keithley function generator (1 V maximum voltage, 0.3 μs rising time, 2.2 μs falling time) on a 10 MΩ resistance. The peak of the two response signals is delayed in time with respect to the input. While the input current reaches its maximum in 0.3 μs, the AD8304 and the LOG114 responses reach their peak in 8 μs and 2.5 μs, respectively. This is not surprising for a LogAmp, but it is interesting to note that, even if both LogAmps are declared to be fast, the LOG114 response reaches its peak in one third of the time of the AD8304.

The fraction of collected charge with respect to the input charge (125 fC) is 83% for the LOG114 (104 fC) and 74% for the

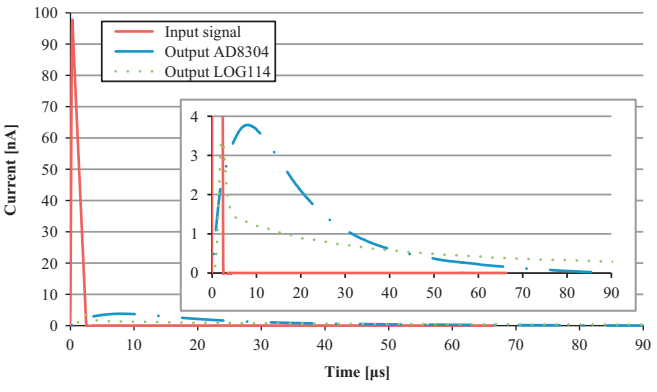


**Fig. 6.** Response of the two LogAmps to the same input current signal.

AD8304 (92 fC) after 90 μs. Thus for both devices the charge collection is fairly slow, especially in the tail, e.g. the LOG114 response is still equal to 10% of the peak value after 90 μs. From this comparison it is clear that the LOG114 is fairly faster in the

first part of the signal, while the charge collection lasts for a longer time as compared to the AD8304. A shorter output signal allows a shorter integration time and a better rejection of the gamma background.

Fig. 7 shows the response of the AD8304 to three different input signals, generated applying a triangular voltage signal on a 1 MΩ resistance. The voltage signal has a rising time of 0.2 μs, a falling time of 1.8 μs and peak values varying from 1 to 5 V, which correspond to a peak current varying from 1 to 5 μA. The AD8304 response is faster if the input current is higher. The peak current of the response is reached in 2.1 μs, 1.4 μs and 0.9 μs for the 1 μA, 2 μA and 5 μA signals, respectively. Consequently if one wants the LogAmp response to become faster, a higher input current must be induced. One way to achieve this is to modify the value of the $I_{min}$ current of the circuit from the nominal value of 200 pA.

Fig. 8 shows the response of the two LogAmps to a single neutron interaction. An AmBe source was placed at 1 m from the instrument and different neutron signals were detected. A full-energy neutron reaction was chosen for each LogAmp to compare signals not affected by wall effects. As already seen for the response to a simulated signal, the LOG114 has a faster response for the first part of the curve. In fact the current peak is at 2 μs for the LOG114 and at 9 μs for the AD8304. Then, after 25 μs the responses are superimposed. This behavior confirms that the LOG114 must be preferred because it describes better the time profile of the current inside the proportional counter. Moreover, higher values of current in the first part of the response lead to a faster response of the LogAmp in the hypothesis that another neutron signal is detected just after the first one. The complete series of electronics tests conducted on the two LogAmps to analyze in details the difference in their behavior can be found in Ref. [20].

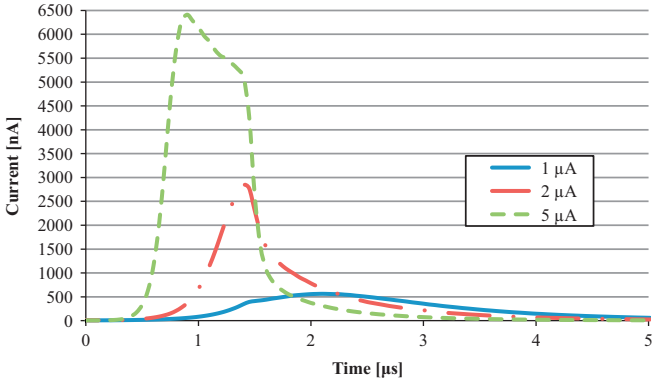


**Fig. 7.** Response of the AD8304 to different input signals, with the same rising and falling times but different peak current.

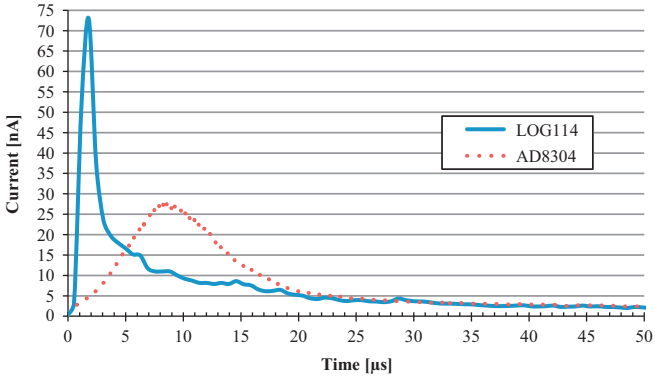


**Fig. 8.** Response of the LogAmps to a single neutron interaction.

From the above results it was decided to employ the LOG114 to improve the performance of the detector in pulsed fields and to reduce the integration time. This has an important impact on the photon discrimination capability. A steady photon field, in fact, produces a steady current superimposed to the neutron signal. The larger the FWHM of the neutron signal, the longer must be the integration time to collect the whole signal and the higher is the contribution to the total charge due to the photons. If this contribution approaches the total charge expected by a neutron interaction, the photon signal can be interpreted as a neutron interaction.

## 3. Experimental results and discussion

### 3.1. Calibration

According to the operating principle of the LUPIN, it is of basic importance to measure the two calibration factors needed to obtain a reading in terms of ambient dose equivalent, H*(10):

- calibration in charge: the MCC.[2] expected from a single neutron interaction, to be used to derive the number of neutron interactions occurring during the integration time, expressed in fC/n and
- calibration in ambient dose equivalent: the conversion coefficient from neutron interactions to H*(10), expressed in nSv/n.

The measurements were carried out in the CERN calibration laboratory with a PuBe source with activity of 1.85 TBq. The operating voltage was set at 1050 V. The output signal was acquired by an ADC with a conversion rate of 5 MSamples/s. This conversion rate was maintained for all the measurements described below.

#### 3.1.1. Calibration in charge

Fig. 9 shows the spectrum obtained after 900 acquisitions. The neutron reaction rate was maintained low enough to avoid multiple neutron interactions in the integration window. The data are shown in terms of number of events per single bin (bin width: 5 fC), where the values on the *X*-axis are expressed as integrated charge over the acquisition time, which was set to 1 ms. The MCC is calculated as the mean of the charge distribution. The value obtained is 229 fC, while the mode of the distribution is 264 fC. The threshold in term of integrated charge was set to 70 fC corresponding to the lower limit of the wall effect continuum. The MCC depends on the type of detector and on the HV polarization, as well as from the acquisition window. Table 1 sums up the value of MCC for each window.

#### 3.1.2. Calibration in ambient dose equivalent

The calibration in ambient dose equivalent was made placing the detector in a radiation field of known intensity and by measuring the number of reactions occurring in a time window of given duration. The uncertainty associated to the reference dose rate was evaluated at 7%, according to the calibration certificate of the PuBe source. The number of reactions occurring in the acquisition window is calculated by the following equation:

$$N = \mathrm{round}\left(\frac{\sum_{i=1}^{n} I_i \Delta t}{Mcc}\right) \quad (1)$$

[2] MCC = Mean collected charge.

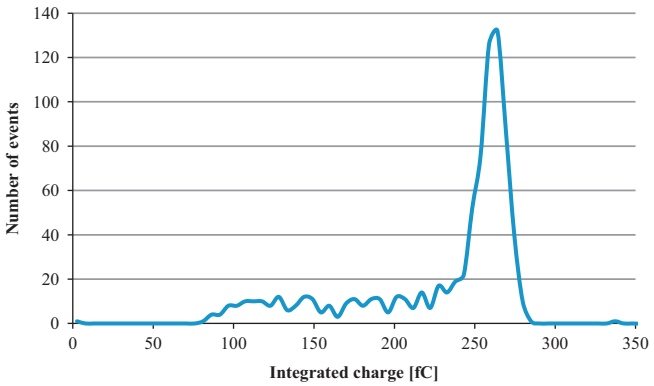


**Fig. 9.** Spectrum obtained with the PuBe source. The *X*-axis values are expressed in integrated charge over the acquisition time (1 ms).

**Table 1**
Values of MCC as calculated for different acquisition windows.

| Time window (ms) | MCC (fC) |
|---|---|
| 0.5 | $211 \pm 15$ |
| 1 | $229 \pm 16$ |
| 2 | $243 \pm 17$ |
| 3 | $251 \pm 18$ |
| 4 | $260 \pm 18$ |

where $N$ is the number of acquired neutrons, "round" is a function which rounds up the number in brackets to the nearest integer number, n is the number of samples in a single acquisition, $I_i$ is the current value of each sample, $\Delta t$ is the time width of the sampling (e.g. for 10 MHz sampling, $\Delta t = 100$ ns) and MCC is given in Table 1.

The detector was exposed at 3 m from the PuBe source. The reference value of ambient dose equivalent rate was 150.52 μSv/h. The calibration factor was determined as $(275 \pm 22)$ pSv/n, where the uncertainty is the sum of two contributions, the one coming from the calibration of the source (7%) and the counting statistics (1%). The sensitivity is about a factor of 4 better than the standard sensitivity of a rem counter (usually close to 1 nSv/count). This meets the requirement 2 given above.

### 3.2. *Measurements at the HZB (Helmholtz-Zentrum Berlin) cyclotron*

The measurements were performed in December 2011 at the Helmholtz-Zentrum Berlin (HZB) using the cyclotron usually employed for proton therapy of ocular tumors. A 68 MeV proton beam was transported to an experimental hall located next to the treatment room. The beam impinged on a cylindrical tungsten target (22 mm in diameter and 20 mm thick) and the LUPIN was placed in the stray neutron field on the beam axis at 50 cm from the target center. The target configuration is shown in Fig. 10.

The cyclotron was operated in pulsed mode, with a repetition rate of 100 Hz, a pulse length of 1–10 μs, and a current on target varying between 2 and 1000 pA. The beam was monitored by measuring the current, whose values were written on a log-file with the corresponding timestamp. The beam settings are listed in Table 2. The burst current is calculated by the following formula:

$$\text{Burst current} = I \text{ on target}/(\text{repetition rate} \times \text{burst length}) \quad (2)$$

The burst charge is the burst current integrated over the burst length. Some of the settings are named with a letter as a suffix

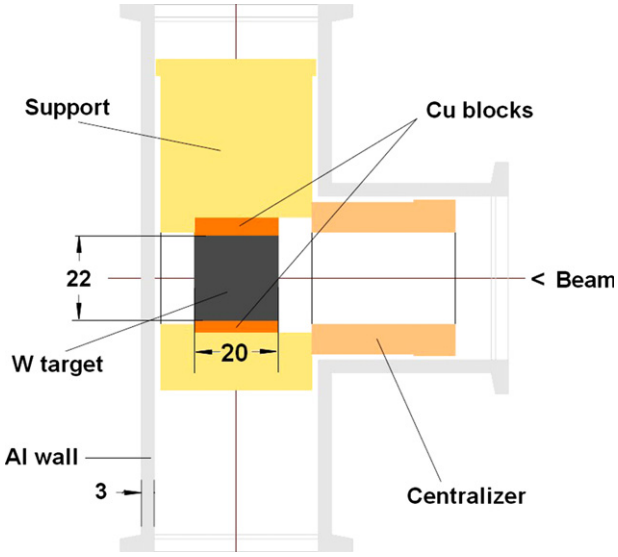


**Fig. 10.** Target configuration at the HZB cyclotron.

**Table 2**
Beam settings used at the HZB.

| Setting number | *I* on target (pA) | Burst current (nA) | Burst length (μs) | Burst charge (fC) | Repetition rate (Hz) |
|---|---|---|---|---|---|
| 1 | 0.2 | 2 | 1 | 2 | 100 |
| 2 | 0.49 | 4.9 | 1 | 4.9 | 100 |
| 3 | 1.07 | 10.7 | 1 | 10.7 | 100 |
| 4 | 2.97 | 29.7 | 1 | 29.7 | 100 |
| 5a | 10.1 | 101 | 1 | 101 | 100 |
| 5b | 10.5 | 105 | 1 | 105 | 100 |
| 6 | 25.3 | 253 | 1 | 253 | 100 |
| 7a | 50 | 500 | 1 | 500 | 100 |
| 7b | 50.6 | 506 | 1 | 506 | 100 |
| 8a | 74.3 | 743 | 1 | 743 | 100 |
| 8b | 74.8 | 748 | 1 | 748 | 100 |
| 9a | 100 | 1000 | 1 | 1000 | 100 |
| 9b | 108.5 | 1085 | 1 | 1085 | 100 |
| 10 | 111 | 111 | 10 | 1110 | 100 |
| 11 | 243 | 243 | 10 | 2430 | 100 |
| 12 | 518 | 518 | 10 | 5180 | 100 |
| 13 | 1000 | 1000 | 10 | 10000 | 100 |

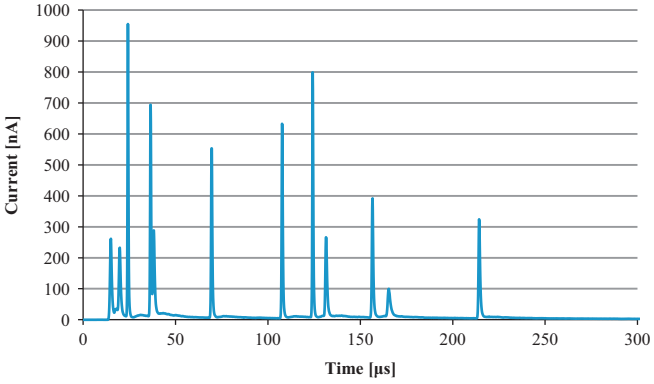


**Fig. 11.** Example of acquisition obtained with the LUPIN with beam setting 9b.

(e.g. setting 5a and 5b) because the machine was set to operate with the same parameters but the obtained currents on target were slightly different.

For comparison the original extended-range neutron rem counter LINUS [15,21–23] was exposed in the same position. The LINUS is a rem counter developed about 20 years ago from an Andersson-Braun

type device. It consists of a $^3$He proportional counter embedded in a spherical polyethylene moderator, which incorporates a boron-doped rubber absorber and a 1 cm thick lead shell so that its response function extends up to several hundred MeV. The electronics was not specifically designed to operate with strongly pulsed radiation: the signal is treated with a standard counting chain (pre-amplifier, amplifier, single channel analyzer and counter) and the TTL counter outputs are acquired by a National Instruments DAQ and analyzed on a laptop.

The aim of the measurements was to check the performance of the LUPIN according to the requirements 1 and 3 above, i.e. its capability to withstand very high instantaneous neutron fluxes with little or no saturation and the capability to measure correctly the intensity of a single neutron burst. The measurements were carried out for the LUPIN with beam settings 5a, 7a, 8a, 9b, 10, 11, 12 and 13; for the LINUS with settings 1, 2, 3, 4, 5b, 6, 7b, 8b, 9a. An example of a single burst acquired by the LUPIN is shown in Fig. 11. The original duration of the proton burst (1 μs) is spread over a few hundred μs due to the thermalization and drift time of the neutrons inside the moderator. Most of the interactions occur in the first 100 μs after the trigger and the rare events in the range 100–300 μs can be ascribed to delayed neutrons. The total charge generated inside the detector is 8.6 pC, corresponding to 36 neutron interactions. Applying the calibration factor, the H*(10) of the radiation burst is 9.9 nSv.

Fig. 12 shows the distribution of the number of neutron interactions per burst on a series of 800 acquisitions with beam setting 9b. During the measurement the cyclotron ion current was particularly steady. The mean value of the distribution is 52.6 neutrons per burst and the variance is 50.6. Hence the variance-to-mean ratio is 0.96. From this result one can say that the number of neutron interactions per burst follows a Poisson distribution.

Fig. 13 shows the acquisition of a single burst delivered with beam setting 13. The contribution from stray radiation is larger, lasting up to 600 μs after the trigger. The distribution of the number of neutron interactions per burst on a series of 500 acquisitions shows a variance-to-mean ratio of 0.5, thus indicating that the distribution does not follow a Poisson statistics. This is consistent with the fact that the LUPIN response is no longer linear and the expected Poisson variation of the random variable (the burst intensity) is reduced.

Fig. 14 compares the LINUS and the LUPIN in term of linearity of their response. For the LUPIN the dose per burst was calculated as the average over a number of acquisitions ranging from 350 to 1000. For the LINUS the dose per burst was calculated as the integral of the dose over 100 s divided by the number of expected bursts. The calibration factor of the LINUS is 0.92 nSv/count.

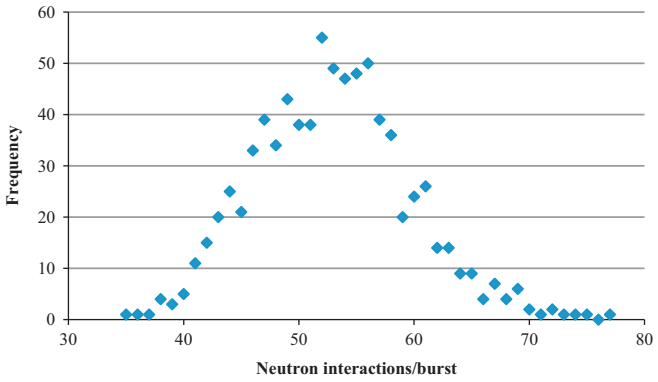


**Fig. 12.** Frequency distribution of the number of neutrons per burst measured with beam setting 9b.

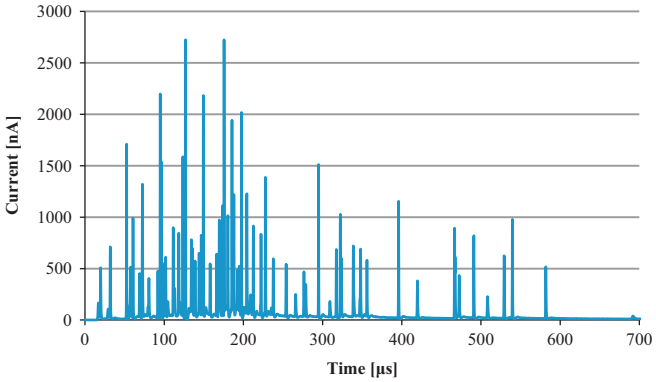


**Fig. 13.** Example of single burst acquisition obtained with the LUPIN with beam setting 13.

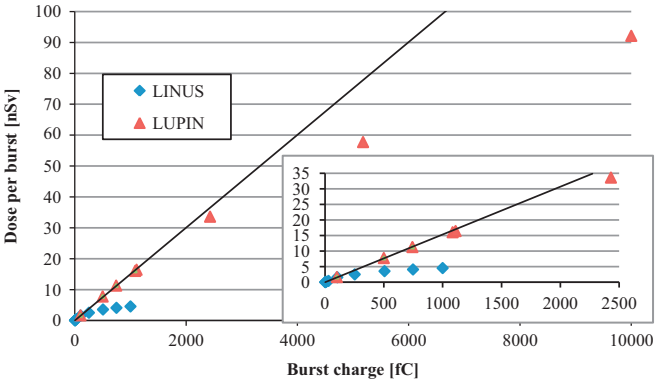


**Fig. 14.** Dose per burst expressed in nSv as a function of the single burst charge. The line shows the fit to the first ten LUPIN data points. The response of the LINUS is plotted for comparison. A zoom of the first part of the graph is also shown.

The LINUS saturates at a few nSv/burst, with the response becoming almost flat. At a burst charge of 1000 fC the LINUS measures an H*(10) value of 5 nSv/burst, underestimating the real dose by 70%. The reliability of the detector is then limited to values below 1 nSv/burst. This is the typical behavior of a detector whose output signal is analyzed by a conventional counting chain without compensation for dead time losses. The response of the LUPIN is linear up to 16 nSv/burst. After this value saturation effects become important. At 58 nSv/burst the underestimation of the dose is 30%, rising to 40% at 92 nSv/burst. This is due to the space charge effect that reduces the electric field between anode and cathode with a consequent decrease of the multiplication factor. This explains the deviation of the distribution of the measured burst intensity from a Poisson distribution, with a variance-to-mean ratio lower by a factor of 2. This effect is similar to the failure of the $X^2$ test for GM counters operating with a counting rate affected by significant dead time losses.

Fig. 14 also shows a linear fit to the LUPIN data acquired at low burst charge, where the saturation effects are negligible. The data in the linear region were used to derive the conversion factor between the dose per burst and the charge per burst, found to be $(15.4 \pm 1)$ nSv/pC at 50 cm from the target. The statistical uncertainties are smaller than the size of the symbol. Applying this conversion factor one can express the $x$-axis in terms of expected dose per burst and the $y$-axis in terms of measured dose per burst. The data expressed with this new reference system are shown in Fig. 15.

Looking at Fig. 15 one can try to express the saturation effect on the H*(10) underestimation via the definition of the parameter $D_{half}$, which is defined as the expected dose per burst at which the detector underestimates by a factor of 2. Appendix A describes

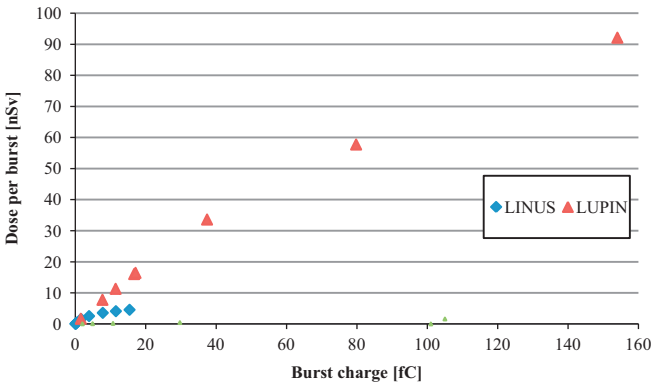


**Fig. 15.** Measured dose per burst as a function of the expected dose per burst, both expressed in nSv, calculated via the conversion factor of $(15.4 \pm 0.1)$ nSv/pC obtained with a linear fit on the first data.

how this parameter has been derived. A correction formula can be applied to compensate for the underestimation. If $D_{meas}$ is the measured dose per burst and $D_{ref}$ is the expected dose, $D_{ref}$ can be derived from $D_{meas}$ by the following formula:

$$D_{ref} = \frac{D_{meas}}{1 - D_{meas}/D_{half}} \quad (3)$$

The parameter $D_{half}$ can be obtained for both detectors via an interpolation of the data of Fig. 15. It is $D_{half}$ (LUPIN)=209.0 nSv and $D_{half}$ (LINUS)=6.3 nSv. Under controlled irradiation conditions the parameter $D_{half}$ can be used to evaluate the instrument capability to withstand a PNF. The higher its value, the better the instrument performs.

### 3.3. Measurements around the PS accelerator complex at CERN

The measurements were carried out in October and November 2011 at the CERN Proton Synchrotron (PS), in three locations selected on the basis of the time structure of the beam losses. The aim was to test the performances of the instrument in different stray field conditions, under operational radiation protection scenarios. The proton beams used for the Antiproton Decelerator (AD), the TOF facility, the LHC and the SPS fixed target physics are extracted from the PS in five turns, using a technique called Continuous Transfer (CT). During this extraction phase, comparatively large losses are observed all around the PS. These losses are due to particles scattered by the electrostatic septum used to slice the beam. The revolution time in the PS is 2.2 μs and the extraction losses are distributed over the entire PS ring, leading to losses of 5–10% of the beam at the energy of 14 GeV/c. The losses are spread over the five turns and therefore have a typical length of about 11 μs. When measuring the losses in a critical point of the PS, one must consider that these 11 μs-losses are always to be added up.

The measurements were performed in the following locations (graphically reported on the PS accelerator complex scheme in Fig. 16):

- *Location* 1: close to beam injection (septum 42). Typical duration of the losses: 200–300 μs, smoothed by the ground shield. Fraction of lost beam: 1–5%.
- *Location* 2: close to beam extraction (septum 16). Typical duration of the losses: 2.1 μs. Fraction of lost beam: 1%.
- *Location* 3: close to beam extraction (septum 16). Typical duration of the losses: 2.1 μs. Fraction of lost beam: maximum about 1%.

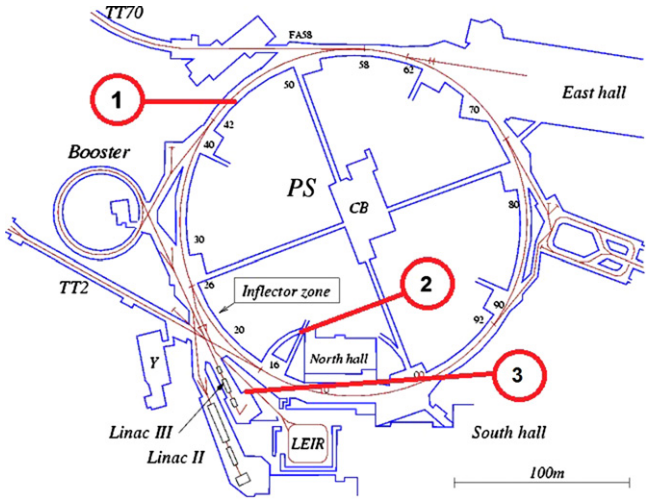


**Fig. 16.** The PS accelerator complex. The small numbers identify some of the PS straight sections. The red marks show the measuring locations discussed in the text (For interpretation of the references to color in this figure legend, the reader is referred to the web version of this article.).

**Table 3**
Measurements carried out at the PS. Integrated ambient dose equivalent measured by the LUPIN and the LINUS, with their statistical uncertainty. The integrated proton fluence and the expected ambient dose equivalent from Monte Carlo simulations (where available) with the FLUKA code are also given.

| Location | Integrated H*(10) (nSv) LUPIN | LINUS | Integrated protons in PS | Expected H*(10) (nSv) (from MC simulations [24]) | |
|---|---|---|---|---|---|
| 1 | $2385 \pm 26$ | | $2310 \pm 46$ | $4.69 \times 10^{15}$ | Not available |
| 2 | $5264 \pm 38$ | | $2879 \pm 51$ | $5.90 \times 10^{15}$ | 5000–6200 |
| 3 | $496 \pm 12$ | | $492 \pm 21$ | $9.82 \times 10^{15}$ | 470–700 |

As can be seen from the typical duration of the losses, the stray radiation field is strongly pulsed in locations 2 and 3. As for the HZB measurements, together with the LUPIN the rem-counter LINUS was exposed for comparison in the same locations. The results of the measurements are reported in Table 3. In Location 1 the results of the LUPIN and the LINUS are consistent within $2\sigma$. As expected, due to the relatively long and smoothed time structure of the beam losses, there are no appreciable count losses due to pile-up or saturation in the LINUS.

In Location 2 the detectors were placed before the interlocked door of the PS access tunnel next to septum 16. The stray field in this area is due to the beam losses in the straight section where the magnetic septum for the beam extraction towards the SPS is located. The access tunnel connects the septum 16 area with the outside, and during machine operation access is possible only up to the interlocked door. An example of a neutron burst acquired with the LUPIN in Location 2 is shown in Fig. 17. The thermalization and drift time of the neutrons inside the moderator spreads the signal over 500 μs. The burst intensity was relatively low, therefore the peak current is limited to 100 nA, while only a few neutrons are delayed in time. The interactions are spread in 500 μs, but the reaction rate is higher in the first 200 μs. The total charge generated inside the detector is 7.1 pC, corresponding to 27 neutron interactions. Applying the calibration factor, the intensity of the radiation burst is 7.4 nSv. The responses of the LUPIN and the LINUS differ by a factor of 2. This is consistent with what can be derived from Eq. (3). In fact, by setting for the LINUS

$D_{helf}$=6.3 nSv and $D_{ref}$=7.4 nSv, one obtains $D_{meas}$=3.4 nSv, i.e. an underestimation of the LINUS by a factor of 2.2, very close to that found experimentally.

Some remarks can be made on the basis of FLUKA [25,26] Monte Carlo simulations available for the area. The PS tunnel is located next to septum 16, where the beam is extracted. Fig. 18 shows the simulated radiation field expressed as H*(10) per primary proton lost on septum 16, towards the exit of the access tunnel [24]. The detectors were placed in an area with an ambient dose equivalent of $0.66 \times 10^{-7}$ pSv/primary lost. At the entrance of the tunnel the H*(10) from gamma contribution is negligible and the field can be completely attributed to neutrons. The beam losses in this region are due to two contributions: 1% coming from the AD, TOF and LHC cycles; 5–10% coming from extraction losses in the overall PS [24]. About 6% of the overall extraction losses of the PS occur at the septum 16 [27], which means an additional contribution of 0.3–0.6% to the total losses. The total fraction of beam which is lost in this area can thus be assumed between 1.3% and 1.6%. The expected ambient dose equivalent is then $(0.86–1.06) \times 10^{-9}$ pSv/primary. Taking into account the integrated proton fluence in the PS (Table 3) during the measurement, an integrated H*(10) in the range 5000–6200 nSv is predicted, in agreement with the value measured by the LUPIN.

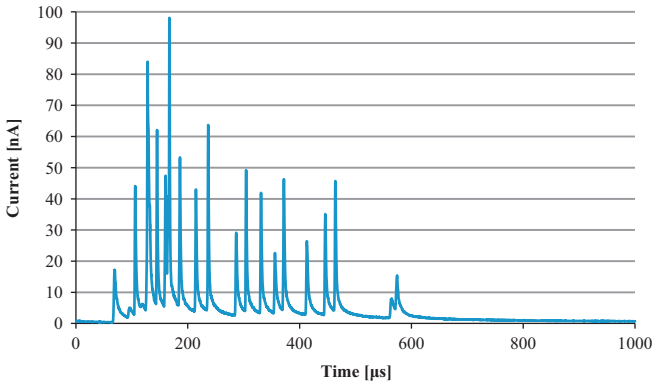


**Fig. 17.** Example of acquisition obtained with the LUPIN in Location 2 at the CERN PS.

In Location 3 the results of the LUPIN and the LINUS are consistent within their statistical uncertainties. To evaluate the reliability of the data, they can be compared to FLUKA Monte Carlo simulations available for the area [24]. It is assumed that most of the dose comes from the neutron component of the stray field. From the simulations it can be derived that, in the position where the instrumentation was placed, the expected ambient dose equivalent is around $(4.1 \pm 0.4) \cdot 10^{-9}$ pSv/primary lost. The same evaluations made for the Location 2 are valid for this area. Assuming that the fraction of the beam lost around septum 16 is 1.3–1.6%, the expected ambient dose equivalent is $(4.8–7.2) \times 10^{-11}$ pSv/primary. Taking into account the integrated fluence in the PS which, from Table 3, is equal to $9.82 \times 10^{15}$ protons, the expected ambient dose equivalent is 470–700 nSv. Taking this value as reference, both the LUPIN and the LINUS results fall within the expected range. In this area, even if the beam losses are characterized by a pulsed structure, both the instruments behave well. This can be explained by the fact that the total losses were really low (dose rate $<100$ nSv/h), so that the electronics of the detectors were not "stressed", in the sense that they may have not been affected by strong dead time. The average value of dose per burst is around 0.5 nSv. In fact in this region (from Fig. 15) both the LUPIN and the LINUS operate in their linear region, without being affected by saturation losses.

As expected the detector readings are coherent where the stray field is characterized by a slow time structure, i.e. in Location 1, or where the stray field is characterized by a very low neutron dose rate, like in Location 3. The differences are severe when the stray field is constituted by a strongly pulsed component, like in Location 2. In this location the Monte Carlo simulations show that the most reliable value of the integrated ambient dose equivalent is the one of the LUPIN, confirming that in these extreme conditions the LUPIN has good reliability if compared to a more conventional instrument. The underestimation of the LINUS can be completely attributed to the dead time losses that affect the electronics during the signal processing.

### 3.4. Measurements at the San Raffaele hospital

The measurements were carried out in January 2012 at the San Raffaele hospital in Milan, using an electron linac employed for

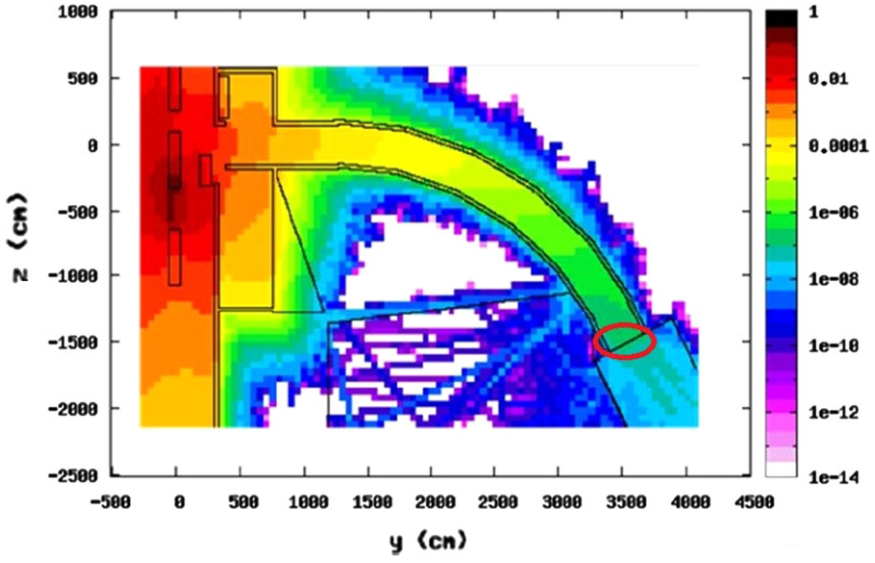


**Fig. 18.** Spatial distribution of H*(10) from a beam loss on septum 16. The results are given as pSv per primary proton lost [24]. The red circle indicates the area in front of the PS access door where the measurements were performed. The H*(10) at this location predicted by the simulations is about $10^{-7}$ pSv/primary lost (For interpretation of the references to color in this figure legend, the reader is referred to the web version of this article.)

radiotherapy. The linac was a Varian Clinac® DHX—Dual energy. It was employed in a fixed irradiation position with the beam directed on the treatment couch, with an irradiation field of $5 \times 5$ cm$^2$. The linac was operating at an intensity of 400 monitor units (M.U.)/min at energies of 6 and 18 MV. The general convention for beam energy specification in photon beam therapy is that the nominal energy refers to the maximum accelerating potential of the electrons incident on the bremsstrahlung target, with the average energy of the photon beam being approximately 1/3 of the maximum accelerating potential [28]. The LUPIN was placed in the patient plane on the treatment couch at a source-to-axis distance of 100 cm, in two different positions, at 32 and 100 cm distance from the isocentre. The measurement set-up is shown in Fig. 19. The aim of the measurements was to test the performance of the LUPIN in terms of reliability of the response in fields characterized by a very intense and pulsed photon component.

Medical accelerators use collimators made of a high-Z absorber to block out portions of the radiation beam. Photons with energies greater than approximately 7 MeV can generate neutrons in interactions with accelerator components, structures in the treatment room and the patient [29]. Most secondary neutrons are generated in the high-Z components of the linac head, i.e. the bremsstrahlung target, collimators and flattening filters [30]. These neutrons then penetrate the head shielding, scatter throughout the treatment room, and are ultimately responsible for undue dose to the patient. The aim of the measurements was to check the behavior of the LUPIN in operational conditions in different stray fields. Firstly in a stray field dominated by photons, generated by the 6 MV beam; secondly in a field characterized by a significant component of secondary neutrons, produced by the 18 MV beam. The response signals obtained at 6 MV at distances of 32 and 100 cm from the isocentre are shown in Fig. 20.

The linac emitted photon bursts at a fixed frequency of around 182 Hz. This value has been derived from a large-window acquisition (10 ms). The signals shown in Fig. 20 are due to photons leaking from the linac head and to scattered photons impinging on the treatment couch. The signal is more than one order of magnitude larger at 32 cm. This is consistent with the decreasing contribution of leakage radiation with increasing distance. The two signals are similar in shape, with the exception of a modulation in the signal acquired at 32 cm. The modulation is characterized by a period of 1.5 μs, i.e. a frequency of 667 kHz.

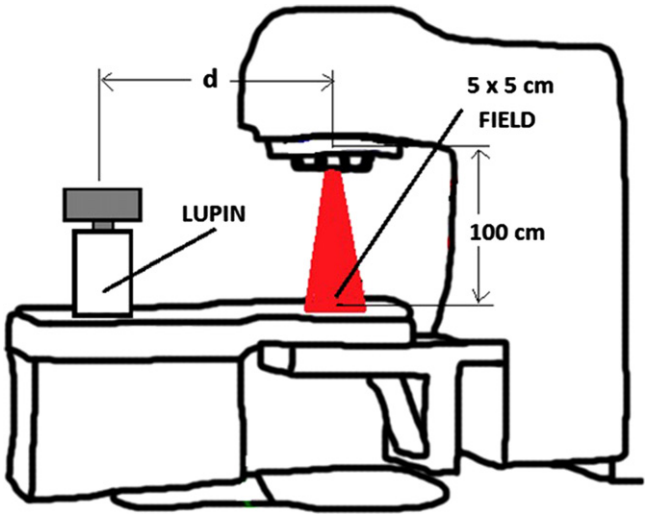


**Fig. 19.** Set-up of the measurements performed at the San Raffaele hospital. The LUPIN was placed at $d=32$ cm and $d=100$ cm. The source-to-axis distance of 100 cm is calculated from the center of the $W$ target located inside the treatment head.

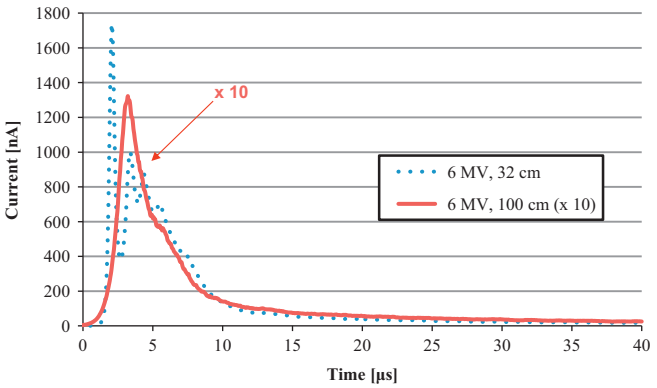


**Fig. 20.** Single-burst acquisitions obtained with the LUPIN at 32 cm and 100 cm from the isocentre at 6 MV. The signal at 100 cm is magnified by a factor of 10.

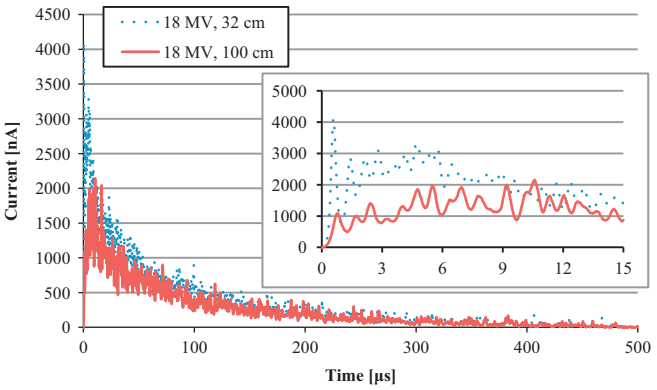


**Fig. 21.** Response signals obtained with the LUPIN at 32 cm and 100 cm from the isocentre at 18 MV. The zoom of the first 15 μs shows the prompt gamma peak.

This modulation can derive from two effects typical of a radiotherapy linac. Firstly, it is known that frequency noise comes from the modulator, with a peak in the power spectral density around 500 kHz [31]. Secondly, radio frequency noise can be produced by the motors of the multileaf collimator, with spikes measured in the power spectral density at 700 and 900 kHz [32]. The total integrated charge for the two signals at 32 and 100 cm is 6.8 and 0.8 pC. This means that the LUPIN detects these signals as if they came from the interactions of 29 and 3 neutrons, respectively.

The detector response at 18 MV is shown in Fig. 21. The signals spread over 500 μs due to the thermalization and diffusion time of the photoneutrons inside the moderator. The interaction rate is higher in the first 50 μs and decreases afterwards, leading to the detection of rare events due to scattered neutrons after 250 μs. A zoom of the response on the first 15 μs shows the peak signal due to the prompt gamma contribution. This contribution is very high in the case of the signal acquired at the 32 cm distance from the isocentre. The difference in the intensity of the signals is less important than at 6 MV, because the signal is mainly due to neutrons, which are isotropically produced in the linac head and uniformly scattered across the room before being detected. The total integrated charge for the 32 and 100 cm acquisitions, excluding from the calculation the gamma contribution under the assumption that it is mostly confined in the first 10 μs, is equal to 145.4 pC and 110.6 pC, respectively, which correspond to 559 and 425 neutron interactions, i.e. 154 and 117 nSv. In this range of measured H*(10) the LUPIN is underestimating. A correction can be applied using Eq. (3) to find out the expected dose per burst. The corrected values are 582 and 226 nSv.

To understand if these values are reasonable one has to compare them with the data available in the literature.

The neutron contamination in a medical electron linac is usually expressed as the ratio between the dose due to secondary neutrons at a given point and the therapeutic photon dose at the isocentre (mSv/Gy). This ratio is obtained by dividing the photon dose delivered in one minute, i.e. 4 Gy (1 M.U.=10 mGy) by the total number of pulses produced by the linac in the same time, i.e. 10920 (182 pulses/s × 60 s). The photon dose rate at the isocentre is thus 366 μGy/pulse. The ratio between the H*(10) due to secondary neutrons at 32 and 100 cm and the photon dose at the isocentre is 1.59 and 0.73 mSv/Gy, respectively.

The H*(10) values heavily depend on the linac design, materials in the head and scattering materials in the room. With the linac operating at 18 MV, recent measurements carried out by means of gold foil activation in Bonner spheres give at 40 cm from the gantry isocentre an H*(10) varying between 0.52 and 1.90 mSv/Gy [28], where the lower value was measured for a Siemens linac and the higher data for a Varian. Via the same technique a value of H*(10) of 0.60 mSv/Gy was obtained for a Siemens linac [33]. Measurements performed via thermoluminescent LiF:Mg, Ti chips placed inside Bonner spheres at distances between 25 and 80 cm from the isocentre gave values of H*(10) independent of the distance and variable between 0.34 and 0.86 mSv/Gy [34]. Higher values were found via measurements with bubble detectors around a Varian Clinac® 2100: the H*(10) varied between 2.3 mSv/Gy at 50 and 100 cm and 10 mSv/Gy at 15 cm from the isocentre [35]. The data agree reasonably well with the present measurements.

As expected the reading of the LUPIN is not reliable when the linac is operating at 6 MV, as the instrument detects the strong gamma burst and interprets it as a signal coming from neutron interactions. Nevertheless, it is interesting to note that one can observe in detail the burst shape, including the internal modulation due to radio frequency noise. At 18 MV the LUPIN measured a considerable amount of neutrons with a dose per burst up to 154 nSv, which, if corrected by an appropriate algorithm, represents a dose per burst up to 583 nSv, in agreement with literature data.

## 4. Conclusions

The capability of efficiently measuring pulsed radiation fields is a challenging task, especially with regard to the neutron component. In the past decades numerous studies focused on the development of detectors specifically conceived to work in pulsed fields. Developments occurred in terms of enhanced response of counters via the use of different technologies. However, a detector meeting all requirements ideally desirable in a survey meter for PNF is still missing: the capability to withstand very high instantaneous neutron fluxes with no saturation, the sensitivity comparable to that of commercially available rem-counters, the capability to measure correctly the intensity of a single neutron burst and the capability to reject the photon contribution. In this study we tested the performance of the new instrument LUPIN via a number of measurements performed under various experimental conditions.

The measurements carried out at the CERN calibration laboratory fixed the settings used in the other experimental conditions in terms of MCC and calibration in ambient dose equivalent. The first parameter is essential for the functioning principle of the LUPIN. The second showed that its sensitivity is about a factor of 4 better than the standard sensitivity of a rem counter, thus meeting the second requirement of an ideal survey meter for PNF.

The tests performed at the HZB showed that the LUPIN response is linear up to an ambient dose equivalent of 16 nSv/burst, with an underestimation of the dose of 40% at 92 nSv/burst. The detector therefore shows the requirements of withstand high instantaneous neutron fluxes with little saturation and of measuring correctly the intensity of a single neutron burst. It was also shown that conventional rem counters heavily underestimate the dose equivalent under the same conditions. Via these measurements a correction algorithm and its critical parameter $D_{half}$ were also derived.

The measurements accomplished at the CERN PS under operational radiation protection scenarios confirmed that the LUPIN response is in the range foreseen by Monte Carlo simulations and that the instrument correctly measures in stray fields consisting of a strongly pulsed component. This confirms the reliability of the detector in terms of capability to withstand very high instantaneous neutron fluxes.

The data acquired around an electron linac proved the reliable behavior of the LUPIN in PNF dominated by a very intense photon component. In fact, even with the presence of a very intense and pulsed gamma field that accompanied the neutron bursts, the detector was able to measure values of H*(10) in agreement with the results reported in the literature for similar accelerators. This confirms that the LUPIN shows the requirement of measuring a PNF rejecting an intense photon contribution that accompanies the neutron field.

The LUPIN proved to meet the four requirements of an ideal survey meter for PNF. According to the results presented in this paper, the detector could be employed in most of operational radiation protection scenarios where PNF are present with good efficiency and reliability. Some limitations are still present in the capability of the detector to withstand very high instantaneous neutron fluxes. In fact the linear behavior of the response has been verified only up to 16 nSv/burst. Moreover, an integrated acquisition system would be desirable, to avoid the need to set the acquisition parameters according to the specific operating conditions.

The limit on the response linearity could be overcome by employing a $BF_3$ proportional counter instead of a $^3$He counter. In fact the sensitivity of a $BF_3$ is lower than the $^3$He and this can reduce the space charge effect that leads to saturation for very intense and pulsed neutron fluxes. In addition, with a good knowledge of the detector response as a function of the dose per burst, under controlled conditions, an algorithm could be implemented in the instrument firmware to further reduce the problems related to the underestimation of the H*(10). The integration of the acquisition system can be achieved by employing a FPGA to acquire the data at a fixed sampling rate. An implementation of a proper algorithm could also allow the user to read from the instrument only the final value in H*(10).

## Acknowledgments

The authors wish to thank Claudio Pirovano for the meticulous work done in mounting the front-end electronics of the first prototype version. The authors also wish to thank Andrea Denker and her colleagues of HZB, Antonella Del Vecchio and the personnel of the San Raffaele hospital who worked overtime to let us perform the measurements. The authors are also indebted to Simone Gilardoni at CERN for useful discussions on the operation of the PS and for his advice on the PS locations where to carry out the measurements.

## Appendix A

The plot of the dose per burst measured by the LUPIN as a function of the expected dose per burst (Fig. 15) shows that,

above a given burst intensity, the instrument saturates and its response flattens. This can be analytically expressed by fitting the response curve with a hyperbola, which has the form:

$$Ax^2+Bxy+Cy^2+Dx+Ey+F=0 \quad (A.1.)$$

where $x$ represents the expected dose per burst and $y$ represents the measured dose per burst, both expressed in nSv. Since there is no quadratic dependence on the response we can put $A=0$ and $C=0$. We also know that if the expected dose is 0, the detector measures *0*, then $F=0$. Eq. (A.1.) then becomes

$$Bxy+Dx+Ey=0 \quad (A.2.)$$

The curve is linear for low values of expected dose per burst, i.e. $y=x$ for $x\approx 0$. Under this condition the term $Bxy$ can be neglected and $D=-E$. Then

$$(B/E)xy - x+y=0 \quad (A.3.)$$

where the ratio $(B/E)$ is constant. We can now introduce the parameter $D_{\mathrm{half}}$ which expresses the expected dose per burst at which the detector underestimates by a factor of 2. This parameter is similar to the dead time $\tau$ in the analysis of dead time losses in a conventional instrument: when the true interaction rate is equal to $1/\tau$, the instrument measures a count rate of $(1/2\tau)$, i.e. it underestimates by a factor of 2.

Thus if $x=D_{\mathrm{half}}$, $y=D_{\mathrm{half}}/2$ it is $B/E=1/D_{\mathrm{half}}$. The measured dose per burst, $D_{\mathrm{meas}}$, as a function of the expected (reference) dose per burst, $D_{\mathrm{ref}}$, both expressed in nSv, is then given by

$$D_{\mathrm{meas}}=\frac{D_{\mathrm{ref}}}{1+D_{\mathrm{ref}}/D_{\mathrm{half}}} \quad (A.4.)$$

$D_{\mathrm{half}}$ is a characteristic feature of each instrument that can be extrapolated from the response curve.

Eq. (A.4.) is very important for the LUPIN because the instrument is capable to detect the intensity of the single radiation burst. This feature makes it possible, once the measured dose $D_{\mathrm{meas}}$ is known, to derive $D_{\mathrm{ref}}$ also under saturation conditions, using the inverse expression. This expression cannot be applied with instruments unable to detect the single burst. Nevertheless, if the time structure of the radiation field is known in term of repetition rate and if the burst intensity can be considered constant, one can apply it to derive the burst intensity and compensate for the dead time losses.

Since the LUPIN measures the individual bursts, Eq. (A.4.) can be embedded into the instrument firmware, without the need of any "a priori" information. Nonetheless, it must be considered that $D_{\mathrm{half}}$ was experimentally assessed with radiation bursts with duration of 1 μs and 10 μs. For longer bursts one can speculate that, if the burst duration is shorter than the neutron thermalization and drift time (about 500 μs), the expression maintains its validity. However, further investigations will be conducted before the algorithm is finally implemented in the instrument firmware.

## References


[1] L. Ruby, J.B. Rechen, Nuclear Instruments and Methods 15 (1962) 74.
[2] L. Ruby, J.B. Rechen, Nuclear Instruments and Methods 53 (1967) 290.
[3] R.J. Lanter, D.E. Bannermann, Review of Scientific Instruments 39 (1968) 1588.
[4] J.W. Leake, T. Lowe, R.S. Mason, G. White, Nuclear Instruments and Methods in Physics Research Section A 613 (2010) 112.
[5] A. Klett, A. Leuschner, Pulsed neutron dose monitoring—a new approach, in: Conference records of the IEEE 2006 Nuclear Science Symposium and Medical Imaging Conference, San Diego, CA, USA, Oct 29–Nov 1, NSS Conference Record, 2, 2007, pp. 806–808.
[6] F.J. Mayer, H. Brysk, Nuclear Instruments and Methods 125 (1975) 323.
[7] D.R. Slaughter, W.L. Pickles, Nuclear Instruments and Methods 160 (1979) 87.
[8] P.M. Dighe, K.R. Prasad, S.K. Kataria, Nucl. Instrum. Meth. A 523 (2004) 158.
[9] M. Luszik-Bhadra, E. Hohmann, Th. Otto, Radiation Measurements 45 (2010) 1258.
[10] M. Luszik-Bhadra, E. Hohmann, A new neutron monitor for pulsed fields at high-energy accelerators, in: Proceedings of the 12th International Congress of IRPA, Buenos Aires, Argentina, 19–24 October 2008, Conference Proceedings, 2009.
[11] W. Weizhen, L. Jianmin, K. Kejun, Nuclear Instruments and Methods in Physics Research Section A 603 (2009) 236.
[12] A. Klett, A. Leuschner, N. Tesch, Radiation Measurements 45 (2010) 1242.
[13] K. Iijima, T. Sanami, M. Hagiwara, K. Saito, S. Sasaki, Progress in Nuclear Science and Technology 1 (2011) 300.
[14] M. Ferrarini, V. Varoli, A. Favalli, M. Caresana, B. Pedersen, Nuclear Instruments and Methods in Physics Research Section A 613 (2010) 272.
[15] C. Birattari, A. Esposito, A. Ferrari, M. Pelliccioni, T. Rancati, M. Silari, Radiation Protection Dosimetry 76 (1998) 135.
[16] M. Cosack, H. Lesiecki, Dependence of the Response of Eight Neutron Dose Equivalent Survey Meters with Regard to the Energy and Direction of Incident Neutrons, Report EUR-7448-EN, 1981, pp. 407–417.
[17] S. Agosteo, M. Caresana, M. Ferrarini, M. Silari, Radiation Measurements 45 (2010) 1217.
[18] N.J. Roberts, D.T. Bartlett, L.G. Hager, L.N. Jones, C. Molinos, R.J. Tanner, G.C. Taylor, D.J. Thomas, Radiation Protection Dosimetry 110 (2004) 187.
[19] Personal Communication of Mr. Andreas Sutter (As-Raydetect-Gmbh, Official Distributor of Centronics for Switzerland), 2011.
[20] G.P. Manessi, Rivelatore attivo per campi di neutroni pulsati, Master Thesis, Politecnico di Milano (in Italian), 2010, pp. 67–85.
[21] C. Birattari, A. Ferrari, C. Nuccetelli, M. Pelliccioni, M. Silari, Nuclear Instruments and Methods in Physics Research Section A 297 (1990) 250.
[22] C. Birattari, A. Esposito, A. Ferrari, M. Pelliccioni, M. Silari, Radiation Protection Dosimetry 44 (1992) 193.
[23] C. Birattari, A. Esposito, A. Ferrari, M. Pelliccioni, M. Silari, Nuclear Instruments and Methods in Physics Research Section A 324 (1993) 232.
[24] S. Damjanovic, T. Otto, Shielding improvements in the region of the ejection septum SS16 of the CERN PS, CERN Technical Note, CERN-SC-2010-022-RP-TN, 2010.
[25] G. Battistoni, S. Muraro, P.R. Sala, F. Cerutti, A. Ferrari, S. Roesler, A. Fasso, J. Ranft, The FLUKA code: description and benchmarking, in: Proceedings of the Hadronic Shower Simulation Workshop, Batavia, IL, USA, 6–8 September 2006, AIP Conference Proceeding 896, (2007) pp. 31–49.
[26] A. Fasso, A. Ferrari, J. Ranft, P.R. Sala, FLUKA: a multi-particle transport code, CERN Technical Note, CERN-2005-10, INFN/TC_05/11, SLAC-R-773, 2005.
[27] M. Caresana, S. Gilardoni, F. Malacrida, G.P. Manessi, M. Silari, Environmental measurements and instrument intercomparison around the PS accelerator complex, CERN Technical Note, CERN-DGS-2012-036-RP-TN, 2012.
[28] R.M. Howell, S.F. Kry, E. Burgett, N.E. Hertel, D.S. Followill, Medical Physics 36 (2009) 4027.
[29] Neutron Contamination from Medical Electron Accelerators, NCRP Report 79, 1984.
[30] S.F. Kry, R.M. Howell, U. Titt, M. Salehpour, R. Mohan, O.N. Vassiliev, Medical Physics 35 (2008) 1906.
[31] M. Lamey, S. Rathee, L. Johnson, M. Carlone, E. Blosser, B.G. Fallone, IEEE Transactions on Electromagnetic Compatibility 52 (2010) 530.
[32] M. Lamey, J. Yun, B. Burke, S. rathee, B.G. Fallone, Physics in Medicine and Biology 55 (2010) 981.
[33] C. Domingo, M.J. Garcia-Fuste, E. Morales, K. Amgarou, J.A. Terron, J. Rosello, L. Brualla, L. Nunez, R. Colmenares, F. Gomez, G.H. Hartmann, F. Sanchez-Doblado, F. Fernandez, Radiation Measurements 45 (2010) 1391.
[34] R. Barquero, R. Mendez, M.P. Iniguez, H.R. Vega, M. Voytchev, Radiation Protection Dosimetry 101 (2002) 493.
[35] F. Vanhavere, D. Huyskens, L. Struelens, Radiation Protection Dosimetry 110 (2004) 607.